P1.1 Lagrangian characterization of terrain induced turbulence based on LIDAR observations: flow characteristics and airplane approaches at Hong Kong International Airport (HKIA)

Wenbo Tang
Arizona State University, Tempe, AZ, USA

George Haller
McGill University, Montreal, Canada

P.W. Chan *
Hong Kong Observatory, Hong Kong, China

1. INTRODUCTION

The Lagrangian descriptions of low-level turbulent airflow motions can be extracted based on fluid particle trajectories from observational data near ground. The primary basis of these descriptions is the Lagrangian Coherent Structures (LCS) revealed by the highlighters of the Finite Domain Finite Time Lyapunov Exponents (FDFTLE). Several other criteria measure the relative motion of trajectories with respect to the LCS. The methodology of LCS extraction and suite of Lagrangian measures for coherent turbulent structures have been developed in Tang et al. (2010a, b). The identified coherent motions can be categorized as updraft, downdraft, horizontal stretching and windshear. The combination of these motions gives rise to various possible flow topologies. Since the Lagrangian measures describe motions relative to an observer moving with the flow, they objectively reflect the wind pattern one would experience when traveling inside the velocity field (such as an airplane).

In Tang et al. (2010b), the different Lagrangian measures are extracted from the two dimensional horizontal wind fields during the passage of a tropical cyclone in April 2008. The wind fields are retrieved using a variational technique from observational data generated by LIght Detection And Ranging (LIDAR) systems situated at the Hong Kong International Airport (HKIA). The Lagrangian measures are compared to the radial velocity of the vertical scans from the LIDAR. It is found that convergences and divergences in the radial direction of the vertical scans compare well with updrafts and downdrafts revealed by LCS. The Lagrangian measures are advantageous as they are objective and provide three-dimensional information on each point in the domain. Additionally, to avoid a very lengthy re-visit time, the vertical scan is only performed at a few isolated azimuthal angles, whereas LCS provide an overview of two-dimensional signature of the three-dimensional airflow structures in the entire measurement domain of the LIDAR. Furthermore, LCS reveals the structures in more detail and with better clarity than streamline plots generated from the two-dimensional wind retrieval shown in Chan and Shao (2007). It is therefore worthwhile to perform LCS extraction on a regular basis to constantly monitor the ever changing turbulent airflow structures surrounding the airport.

* *Corresponding author address:* P.W. Chan, Hong Kong Observatory, 134A Nathan Road, Hong Kong email: pwchan@hko.gov.hk

Our interest is not just centred on the airflow structures. The more important question is how will these coherent structures affect airplanes during take-offs and landings. One hazard to identify is significant low-level windshear appearing as strong headwind change over short distances, as it changes the lift of aircraft. Also of interest would be updrafts and downdrafts of airflow as they directly exert vertical forcing on an aircraft and suddenly change its altitude. Indeed in aviation industry the two quantities are combined to form the “F-factor”, which serves as an index for changing performance of an aircraft (Proctor et al. 2000). In the context of Lagrangian analyses, highlighters of the FDFTLE field reveal strongest nonlinearity of a flow field, which bring forward the strongest change of relative motion of airflow. This change of velocity structures is correlated to onboard data during low-altitude low-speed operations to understand what an airplane experiences when flying through such a velocity field.

We have collected data from airplane landings for a tropical cyclone case in 2008. The landing data include those directly measured by sensor onboard, such as horizontal wind speed and direction, as well as data processed by software that considers aerodynamic parameters, such as the airplane altitude, vertical wind velocity, F-factor and eddy dissipation rate. We compare vertical and horizontal motions indicated by LCS with turbulence experienced by airplanes to seek possibility of operational use of LCS in hazard detections.

2. COHERENT STRUCTURE EVOLUTION

In this section we study the evolution of LCS. LCS is first extracted as highlighters of the FDFTLE fields. Lagrangian versions of horizontal divergence (DIV), shear (SHR) and strains normal and parallel to the LCS are computed along the trajectories to categorize the motion each FDFTLE highlighter is associated with. LCS extraction is performed consecutively at 150 second intervals to monitor the change in shape and location of the coherent structures.

Some aspects of the 19 April 2008 case have been discussed in Tang et al. (2010b) to demonstrate the Lagrangian measures. This episode refers to a tropical cyclone which made landfall over western coast of southern China and moved inland in a northeastern track. This brought rain bands and strong southerly winds near the Airport. Turbulent flow structures arise when this southerly flow climbs over the terrain south of the HKIA. Lagrangian

analyses were performed between 1430 UTC and 1500 UTC to study the evolution of flow structures associated with this cyclone. In Tang et al. (2010b), we have seen that the southerly winds associated with the tropical cyclone passing over mountain ranges south of the airport generate hairpin structures at the southwest corner of the analysis domain. In fact, these structures periodically shed small patches of velocity anomalies which are advected with the background flow. The evolution of such a shedding is captured at 1441 UTC, 19 April 2008.

Figure 1 shows the overall conditions of coherent structures at 1441 UTC, 19 April. Black iso-contours are the topography in the airport region, shown at 100 m intervals. The airport island is located at the centre of the figures. The color maps are the FDFTLE fields extracted from forward-time (Figure 1(a)) and backward-time (Figure 1(b)) trajectories. Highlighters of FDFTLE are in red, which correspond to the largest fluid trajectory separation over time and therefore are the LCS we look for. Superimposed in the plots are the white DIV iso-contours at 90th percentile (values in the caption), showing strong vertical motions. In general vertical motions, appearing as updrafts and downdraft, are associated with the LCS.

Since this time is only 12 minutes after the data analyzed in Tang et al. (2010b), the flow share similar features. A couple of hairpins are identifiable near the 'X's marked at the corresponding mountain peak and ridge which give rise to these structures. The shape of the left hairpin is undergoing strong deformation which in fact is associated with the structure shedding. This hairpin is highlighted in the black ellipse in Figure 1(b). To the right of this plot, a long ridge is seen to last over time.

In addition to extracting LCS, we also plot Hovmöller diagram to compare shedding flow structures. Figure 2 shows this diagram between 1400 UTC and 1600 UTC. In Figure 2(a), the LOS velocity is shown between the 214° azimuth and 240° azimuth, in 1 degree intervals, at 6 km range from the LIDAR. There are two streaks of velocity bubbles indicating reversal flow near 220° and 225° azimuth. They seem to indicate periodic shedding of velocity structure near these angles at around 20 minute intervals.

We also plot the Hovmöller diagram at different range from the LIDAR for a fixed angle of 225° in Figure 2(b). We notice a persistent anomaly at 6 km from the LIDAR, with velocity bubble period of roughly 20 minutes. These diagrams are similar to the findings in Shun et al. (2003). In addition, as discussed in Chan and Shun (2005), structure shedding in a stable boundary layer condition near HKIA tends to have shedding period between 15-45 minutes. The Hovmöller diagram and the LCS analyses both point to a shedding frequency consistent with their findings.

3. AIRPLANE LANDING STUDIES

During the tropical cyclone event, several flights conducted missed approach procedures and landed successfully later due to windshear/turbulence. We present one such case in this section, containing one unsuccessful and one successful landing.

The landing was conducted at 1346 UTC, 19 April 2008, using 25R (landing at the northern runway of HKIA from the east). We present in Figure 3 the analyses of LCS with the landing record. In Figures 3(a) and 3(b), a 3D view of the airport is seen from the southeast. Here the horizontal axes are longitude and latitude, in degrees, and the vertical axis is height, in meters. The color map in the centre denotes forward-time FDFTLE in (a) and backward-time FDFTLE in (b). To differentiate repellers from attractors, we use the negative value of backward-time FDFTLE such that red ridges correspond to downdrafts in (a) and blue ridges correspond to updrafts in (b). These color maps are plotted at the respective height of the LIDAR scanning angle (1.4°), and thus the surface is a cone, where the tip of the cone is the location of the LIDAR, highlighted by the black dot.

Next to the LIDAR, the northern and the southern runways are highlighted as thick black lines. For this flight landing from the east, the approaching trajectory is highlighted as the thin solid line. This trajectory is not exactly following the LIDAR cone (because of the approaching angle being 3° and the target being the runway threshold), thus we project the approaching trajectory onto the cone with an additional black solid line, so one can visually compare the coherent structures with airplane landing data. Finally, the airplane records various parameters among which the vertical wind component is derived. We plot and compare the time rate of change of the vertical wind velocity as an indicator of airplane experiencing significant up/downdraft as the white curve above the landing trajectory. A reference value of 0 is also plotted as a white line so one can identify updraft from downdraft.

From these 3D views, one can develop a sense of the correlation between downdrafts and the red ridges as well as updrafts and the blue ridges. To elaborate this correlation, we plot in Figure 3(c), the vertical acceleration scaled by a factor of 20 in the black solid line, compared with FDFTLE interpolated along the plane trajectory. The horizontal axis is nautical miles and the vertical axis is variable dependent on the curves. The red and blue lines in Figure 3(c) denote forward-time and backward-time FDFTLE, respectively, with the forward-time FDFTLE plotted in its negative value. As such, peaks in blue lines indicate updrafts and troughs in red lines indicate downdrafts. Here the solid lines of FDFTLE are derived from 1.4° scans and the dashed lines are derived from 3.0° scans. Since the plane trajectory is closer to the 3.0° scans at the beginning of descent, we should compare the vertical acceleration with 3.0° scans further away from the LIDAR. For the FDFTLE curves, since only the peaks and troughs are important in their relation to the up/downdrafts, we filter FDFTLE values at threshold 0 for visual convenience.

It is found for this approach that the updrafts and downdrafts derived from airplane data correlate well with the defining signatures of LCS — the extrema of the FDFTLE fields. As an additional

comparison, we plot the head wind profile measured from the airplane and derived from the 1.4° scan. (Note that there is an operational headwind profile generating pattern employed at HKIA, which follows exactly the 3.0° descending angle along the runway corridor. This operational headwind profile is not used here as it is a single line of data which cannot be used to derive the Lagrangian measures.) Although the headwind profile from the 1.4° scan lacks small-scale variability as compared to plane data, it does in general follow the trend.

4. CONCLUSIONS

We have used the set of tools developed in Tang et al. (2010a, b) to study the evolution of airflow structures near HKIA. We have found structure generation and shedding from patches of velocity anomalies aloft mountain peaks and ridges. These dynamical pictures of the airflow structures around the airport provide useful indication of aviation hazards for weather forecasters.

To further understand the interaction of the airflow structures with aircraft, we analyzed landing data obtained onboard the aircraft, and compared with the LCS we extract from variational wind retrievals based on LIDAR on the ground. It turns out that there is in general good correlation between extrema of FDFTLE, which are the location of the LCS indicating the most unstable air motion, and up/downdrafts from derived vertical acceleration of atmosphere, indicating jitters experienced by the aircraft. This agreement is dependent on the correlation between the headwind profile measured from onboard sensors and that derived from the LIDAR outputs.

Further studies would be carried to determine if there is any quantitative correlation between the extrema of FDFTLE and the vertical acceleration. For this purpose, a larger amount of aircraft data collected under different weather conditions would be considered. The study results would be reported in the papers in the future.

References

Chan, P. W. and A. M. Shao, 2007: Depiction of complex airflow near Hong Kong International Airport using a Doppler LIDAR with a two-dimensional wind retrieval technique. Meteorol. Z., **16**, No. 5, 491-504.

Chan, P. W. and C. M. Shun, 2005: Numerical simulation of vortex shedding observed at the Hong Kong International Airport using a shallow water model. Croatian Meteorological Journal, **40**, 27–30.

Proctor, F. H., D. A. Hinton, and R. L. Bowles, 2000: A windshear hazard index. Preprints of 9th Conference on Aviation, Range and Aerospace Meteorology, Orlando Florida, American Meteorology Society, 482–487.

Shun, C. M., S. Y. Lau, and O. S. M. Lee, 2003: Terminal Doppler weather radar observation of atmospheric flow over complex terrain during tropical cyclone passages. J. Applied Meteorol., **42**, 1697-1710.

Tang, W., P. W. Chan, and G. Haller, 2010a: Accurate extraction of Lagrangian coherent structures over finite domains with application to flight data analysis over Hong Kong International Airport. Chaos, **20**, 017 502.

Tang, W., G. Haller, and P. W. Chan, 2010b: Lagrangian coherent structure analysis of terminal winds detected by LIDAR, Part I: turbulence structures. J. Appl. Meteorol. Clim., submitted.

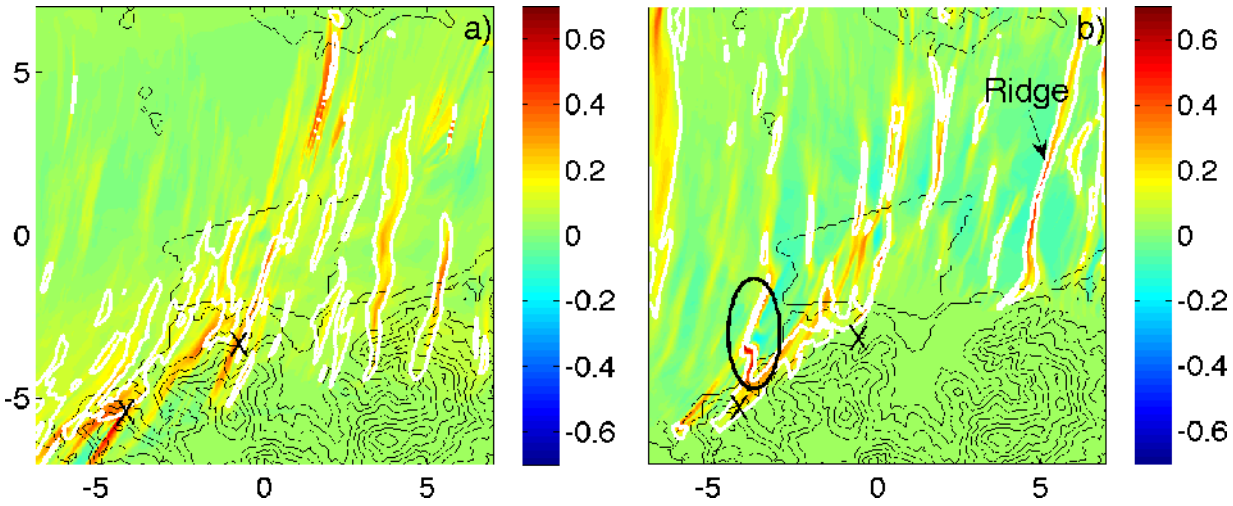

Figure 1 Lagrangian Coherent Structures obtained at 1441 UTC, 19 April 2008. (a) Forward-time FDFTLE field. Maximizers indicate repelling structures. The white iso-contours correspond to DIV with value of 0.09. (b) Backward-time FDFTLE field. Max-imizers indicate attracting structures. The white iso-contours correspond to DIV with value 0.06. Hairpin structures next to mountain peaks and ridges are marked by 'X's. Black ellipse in (b) indicates a region of structure shedding. A persistent ridge of updraft is identified as well. The unit of the axes is kilometres. The unit of the colour maps is min^{-1}.

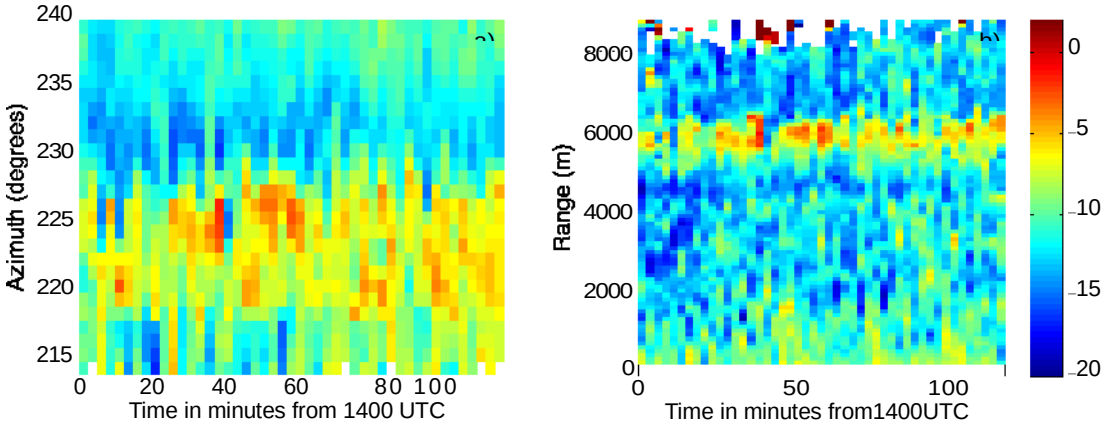

Figure 2 Hovmöller diagram taken with the 1.4° LIDAR scan between 1400 UTC and 1600 UTC on 19 April 2008. (a) Azimuthal angles from 214° — 240° at range 6 km from the LIDAR. (b) Azimuthal angle of 225° for different ranges from the LIDAR.

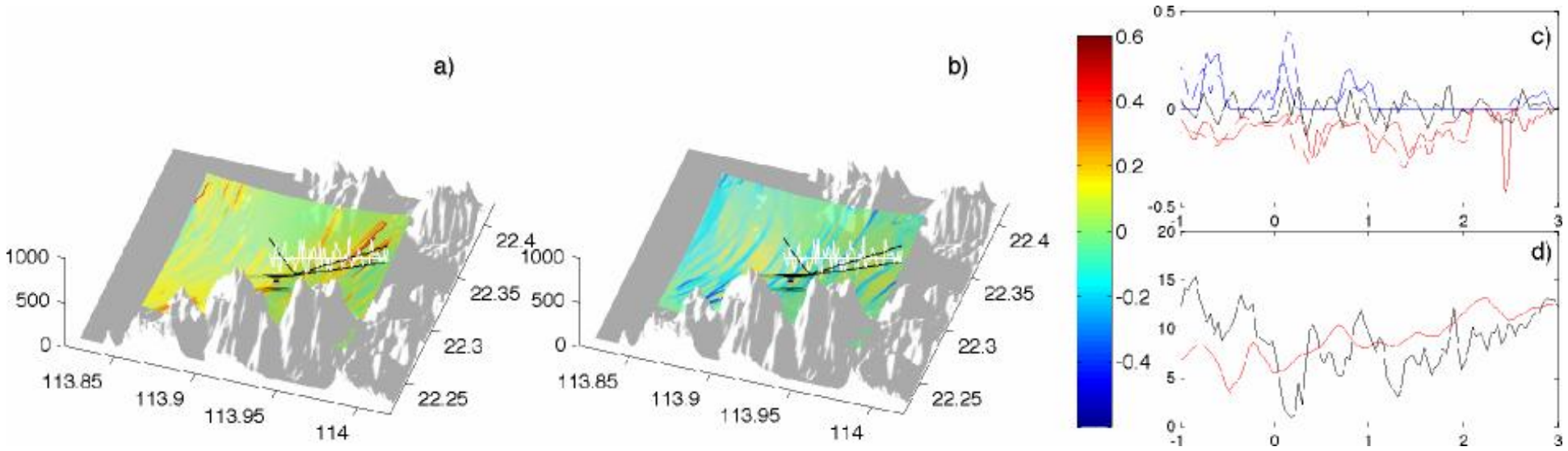

Figure 3 Airplane landing data compared to LCS for missed approach at 1346 UTC, April 19th, 2008. (a) Approach superimposed on forward-time FDFTLE. The shaded topography indicates nearby mountainous terrain near HKIA. The color map is the forward-time FDFTLE plotted at the 1.4° LIDAR cone with the LIDAR highlighted at the tip of the cone. Thick black lines denote the two runways. Thin black lines denote approaching trajectory and its projection on the LIDAR cone. The white curve is acceleration of vertical velocity derived from onboard sensor. The flat white line is a reference line of 0. (b) Approach superimposed on backward-time FDFTLE. All styles same as (a). (c) Comparison between vertical acceleration (black) and FDFTLE. The blue/red solid lines are the backward/forward-time FDFTLE generated from the 1.4° scan, with forward-time FDFTLE plotted in its negative value (so troughs of red lines indicate locations of downdrafts and directly compare to troughs of vertical acceleration; peaks of blue lines indicate locations of updrafts and directly compare to peaks of vertical acceleration). The dashed lines are generated from the 3.0° scan. (d) Comparison between headwind generated from onboard sensors (black) and derived from LIDAR outputs (red).